

A Wireless Batteryless Deep-Seated Implantable Ultrasonic Pulsar-Receiver Powered by Magnetic Coupling

Sai Chun Tang, Ferenc A. Jolesz, and Gregory T. Clement

Abstract—This study tests a deep-seated implantable ultrasonic pulsar-receiver, powered wirelessly by magnetic coupling. A 30-cm energy-transmitting coil was designed to wrap around the body, and was driven by a current of 1.2 A rms at a frequency of 5.7 MHz to generate a magnetic field. A 2-cm receiving coil was positioned at the center of the primary coil for receiving the magnetic energy and powering the implantable device. A capacitor-diode voltage multiplier in the implantable circuit was used to step-up the receiving coil voltage from 12.5 to 50 V to operate an ultrasonic pulsar. FEA magnetic field simulations, bench-top, and *ex vivo* rabbit measurements showed that the magnetic energy absorption in body tissue is negligible and that the magnetic coupling is not sensitive to receiving coil placement. The receiving coil and the power conditioning circuits in the implantable device do not contain ferromagnetic material, so a magnetic-resonance-compatible device can be achieved. A 5-MHz ultrasound transducer was used to test the implantable circuit, operating in pulse-echo mode. The received echo was amplified, envelope-detected, frequency-modulated, and transmitted out of the rabbit body by a radio wave. The modulated echo envelope signal was received by an external receiver located about 10 cm away from the primary coil. The study concludes that operation of a batteryless and wireless deep-seated implantable ultrasonic pulsar-receiver powered by coplanar magnetic coupling is feasible.

I. INTRODUCTION

ADVANCES in microelectronics and medical technologies have prompted research efforts on developing implantable devices for diagnosis [1]–[5]. Such devices, once encased in biocompatible materials, are designed to stay in the body indefinitely. In ultrasound, implantable devices have the potential to monitor deep-seated tissues; particularly those that are unreachable using external devices because of proximity to air or bone [6]. This potential has motivated a variety of studies on applications of implantable ultrasound devices for diagnosis [1]–[4].

One such application is designed for use as a blood-flow monitor in artificial vascular grafts, to extend the life of the graft [4]. This device uses a specially-designed transducer embedded in the wall of an artificial graft to monitor the graft flow daily and communicate to a physician if the flow suggests impending failure. Another application is aimed at monitoring patients with chronic heart diseases [1]–[3]. The implantable device in this application

monitors a patient's hemodynamic function, such as heart chamber volume and blood flow velocity. The ultrasound transducer can be positioned close to [1] or inside [2], [3] the heart, and is powered by embedded batteries which require replacement after several years.

In addition to previously-studied applications, there are clearly potential uses that have yet to be realized. One such application, which has motivated the present study, is the use in monitoring organs after transplant surgery. For example, after renal transplantation there is risk of acute rejection [8]–[11] or thrombosis of the renal artery [12]. Acute thrombosis occurs hours or days after surgery; kidney rejection commonly occurs within the first few weeks after kidney transplantation and is uncommon after the first year [9]. Here, implantable ultrasound could potentially be used to detect the diameter decrease (thrombosis) or increase of the deep-seated renal artery, which is regarded as a sign of acute renal rejection.

Arguably, the most challenging aspect of designing a deep-seated implantable device is providing a long lasting and reliable power source for the device. Percutaneous plugs, wires, or conduits can deliver power, but the treatment pierces the patient's skin and increases the risk of infection [13]. Another method entails embedding a battery in the implantable device to avoid the problems associated with the percutaneous parts, but the battery could be a barrier to device miniaturization [14]. Moreover, the lifetime of a battery is limited and a battery replacement surgery is required after several years. Wireless energy transfer using a transcutaneous transformer is preferred for reliability in long-term implantable devices because it eliminates the drawbacks of the previous methods [13]–[18]. However, there are still many difficulties in using the transcutaneous transformer, because the magnetic field coupling coefficient is diminished by the transformer air gap, which is determined by the thickness of the patient's skin and subcutaneous fat [18]. The transformer primary coil, positioned outside the body and connected to an external driving circuit, is used to generate a time-varying magnetic field. The secondary coil is located inside the body and connected to the implantable circuit, which is used to receive the magnetic field and convert it to electrical energy for powering the implantable circuit. The two coils are coaxial and facing each other, so the magnetic coupling coefficient is sensitive to the variation of the coil separation and misalignment [15], [16]. Unfortunately, the air gap is not constant and the induced voltage at the receiving coil varies during operation [18]. Moreover, be-

Manuscript received October 20, 2010; accepted March 19, 2011.

The authors are with Brigham and Women's Hospital/Harvard Medical School, Radiology, Boston, MA (e-mail: sct@bwh.harvard.edu).

Digital Object Identifier 10.1109/TUFFC.2011.1931

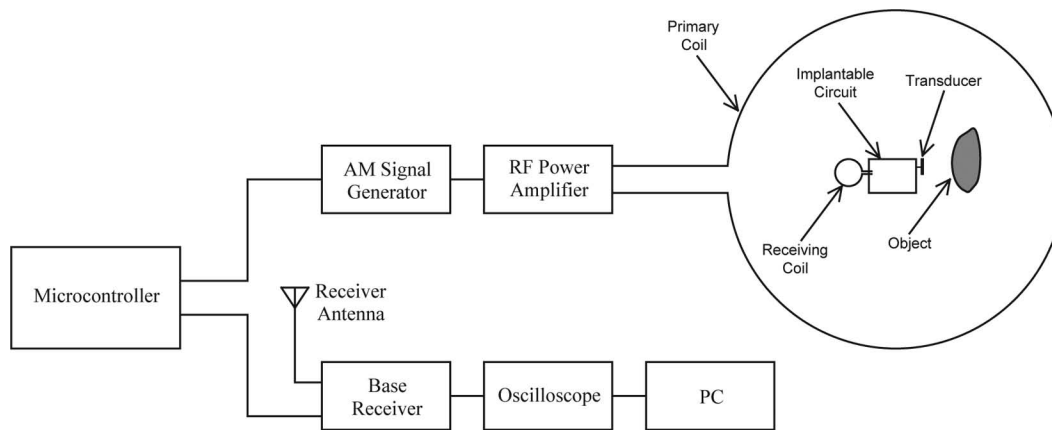


Fig. 1. A block diagram of the pulser-receiver system.

cause the magnetic coupling and power transfer efficiency of a transcutaneous transformer drop proportionally with the coil separation [14], [19], the depth of an implantable device could be significantly limited.

In this paper, a different approach is used to deliver sufficient power to operate an implanted ultrasonic pulser, receiver, and transmitter. The primary loop is designed to wind around the body. The secondary coil is positioned on the plane, and at or around the center of the primary loop. In this configuration, the secondary coil is naturally deep-seated in the body to power the implantable circuit. The diameters of the primary and secondary coils are 30 cm and 2 cm, respectively. Thus, the separation between the two coil wires is 14 cm, which is much larger than that provided by commonly used face-to-face type transcutaneous transformers. This wireless approach may provide a long-term and reliable power source for implantable ultrasound devices for monitoring chronic diseases or acute organ rejection. Along with the general evaluation of this approach, we introduce a new implantable device, which was developed and evaluated as part of this study.

The problem of magnetic energy absorption in body tissue, which is proportional to the magnetic field frequency, is considered in the system design. It was found that magnetic energy absorbed by body tissue at a magnetic field frequency of 12 MHz was 1.5% of the transmitted energy [20]. At higher frequencies, the absorption rate is higher. In our prototype design, the magnetic field frequency is chosen to be 5.7 MHz with the consideration of the bandwidth, linearity, and stability of the RF power amplifier, and the limited available values of the low-loss capacitors C_r in the LC resonance network in the energy receiving circuit. Finite-element-analysis (FEA) simulations and animal experiments are performed to verify the energy absorption by conductive body tissue is negligible at this frequency and would not significantly affect the amount of energy transferred to the receiving coil, such that the implantable device could be powered by the primary with a reasonable current level. The FEA simulation is also used to analyze the magnetic field intensity

distribution and the receiver coil output signal sensitivity to coil placement error.

The receiving coil used in this study has no ferromagnetic core, and the power converter circuits in the implantable device do not contain inductors. This has particular importance for magnetic resonance (MR) compatibility, because the implanted device does not contain ferromagnetic material. This may be contrasted with the use of transcutaneous transformers for power delivery.

The operating principle of the implantable device is outlined in this paper. The induced voltage at the receiving coil is converted to the desired voltage levels for supplying power to different parts of the device. The operating sequence of the device is determined by a microcontroller unit. A 5-MHz ultrasound transducer is used to convert electrical energy from the pulser to an acoustic wave and also to convert the acoustic echo back to an electrical signal. The echo signal is amplified, envelope-detected, frequency-modulated (FM) onto a carrier, and transmitted out of the body through a monopole antenna. An external receiver circuit is developed to demodulate the FM signal. From the recovered signal obtained at the external receiver output, an object can be wirelessly monitored and the distance between the transducer and the object evaluated.

II. WIRELESS ENERGY TRANSFER AND MAGNETIC FIELD DISTRIBUTION

The wireless energy transfer is based on magnetic field coupling from a primary coil that wraps around the human body to the secondary receiving coil implanted inside the body to power the implantable circuit. The secondary coil, which is located on or near the plane of the primary coil, receives the time-varying magnetic energy and converts it to electrical energy by electromagnetic induction. A block diagram of the system is shown in Fig. 1. In the diagram, the amplitude modulated (AM) sinusoidal current exciting the primary coil is generated by a signal generator (33250A, Agilent Technologies, Santa Clara, CA)

and amplified by an RF power amplifier (240L, Electronics & Innovation, Rochester, NY). The carrier frequency of the AM signal is set to 5.7 MHz in the prototype system. The primary coil has a single turn in an approximately circular shape with a diameter of 30 cm and is designed to surround the waist of a human body. The coil is made of a copper wire with a diameter of 0.5 mm.

The magnetic field intensity expected by the primary coil was simulated by FEA using Ansoft Maxwell in 3 dimensions (Ansys Inc., Canonsburg, PA). In the simulation, the primary coil wound around a cylinder filled with a material that has the same conductivity as physiological saline ($1.4 \text{ S}\cdot\text{m}^{-1}$) [21], to approximate the conductivity properties of the human body. A controlled simulation experiment with air replacing the conductive material in the cylinder was performed to compare the effects of the conductivity of human tissues on the magnetic energy absorption and energy transfer. The magnetic field was simulated in a cylindrical boundary with a diameter of 1 m and a height of 2 m, and the primary coil was located at the middle of the cylinder filled with air. Fig. 2 shows the magnetic field intensity, along the coil's axial (z -axis) and the radial (x -axis) directions, induced by the primary current of 1 A rms at 5 MHz. Because the magnitude of the magnetic field is symmetric about the coil center, the plots in Fig. 2 only show the fields in the positive sides of the axes. With the controlled simulation, the magnetic field plots show that the impact of the conductive tissue on the attenuation of the magnetic field is negligible, because the frequency of the magnetic field is less than 12 MHz [20]. In Fig. 2(a), the maximum magnetic field intensity is located at $z = 0$, i.e., on the plane of the primary coil, and the magnetic field intensity decreases slowly as z increases from 0 to about 2 cm. When z increases further (from about 2 cm), the magnetic field intensity reduces rapidly. The field intensity drops from 97% of its maximum at $z = 2$ cm to 35% at $z = 15$ cm (distance equivalent to one radius of the coil). This phenomenon implies that optimization of magnetic field coupling, and hence energy transferring to the implantable device, can be achieved by placing the secondary receiving coil on or near the primary coil plane. Also, from the result, we can see that this arrangement allows a few centimeters of coil placement error in the direction normal to the primary coil plane.

From the simulation in Fig. 2(b), it is predicted that the magnetic field on the plane and around the center of the primary coil is relatively even and does not vary significantly compared with that near the coil. The variation of the magnetic field within a region of 10 cm diameter at the center of the primary coil is less than 10%. It is then predicted that when the secondary coil is placed on the plane and near the center of the primary coil, the coupled magnetic field and induced voltage in the receiving coil are more predictable and less sensitive to the coil placement error in the direction parallel to the primary coil plane.

Aligning the primary coil with the receiver coil is required because the output voltage of the receiver coil drops

proportionally to the cosine of the angle between the axes of the coils. If such alignment is not feasible, three receiving coils with mutually orthogonal axes could be utilized.

III. IMPLANTED CIRCUIT DESCRIPTION

A. Energy Receiving

A 2-cm-diameter secondary coil with 5 turns is used to receive the magnetic energy and convert it to electrical energy. Unlike traditional transcutaneous transformers, which utilize ferromagnetic core [18] to transfer energy to the implantable devices, the receiving coil used in the proposed implantable device does not utilize ferromagnetic material, allowing the implantable device to be MR-compatible. The secondary coil is made of a copper wire with a diameter of 0.5 mm, its inductance, measured at 5 MHz using an HP4194A impedance analyzer (Hewlett-Packard, Santa Clara, CA), is 802 nH, and its quality factor is 130. A resonance technique is used to significantly increase the received voltage by connecting a high-frequency, low-loss capacitor, C_r , in parallel to the secondary coil as shown in Fig. 3. The receiving network resonant frequency, which is selected to be the same as the primary current frequency (5.7 MHz) to achieve maximum energy transfer, is given by

$$f_r = \frac{1}{2\pi\sqrt{L_r C_{eq}}}, \quad (1)$$

where L_r is the inductance of the receiving coil, and C_{eq} is the equivalent capacitance of the capacitor C_r in parallel with the resulting capacitance of the voltage converter and the junction capacitance of the rectifier diodes. Because the equivalent capacitance of the voltage converter and the rectifier is about 150 pF and the inductance of the receiving coil is 802 nH, from (1), the required capacitance value of C_r is 820 pF to achieve a resonant frequency of 5.7 MHz.

B. Power Conditioning

The rectified voltage from the LC resonant circuit is about 12.5 V when the receiving coil is placed at the center of the primary coil. The supply voltage for the MOSFET driver circuit is set to about 8 V. Because the pulser circuit requires a voltage level of about 50 Vdc to generate a 50 V pulse for the ultrasound transducer excitation, a $4\times$ voltage multiplier is needed to step up the receiving coil voltage. Fig. 4 shows a 2-stage Greinacher cascade voltage multiplier that steps up and rectifies the receiving coil voltage to about 50 Vdc. Other parts of the implantable circuit require lower voltage levels. A step-down voltage converter made of energy-efficient capacitive voltage dividers is used to step down the coil voltage to about ± 6 V (Fig. 5). Low-dropout linear voltage regulators are used to adjust the voltage to the desired levels for differ-

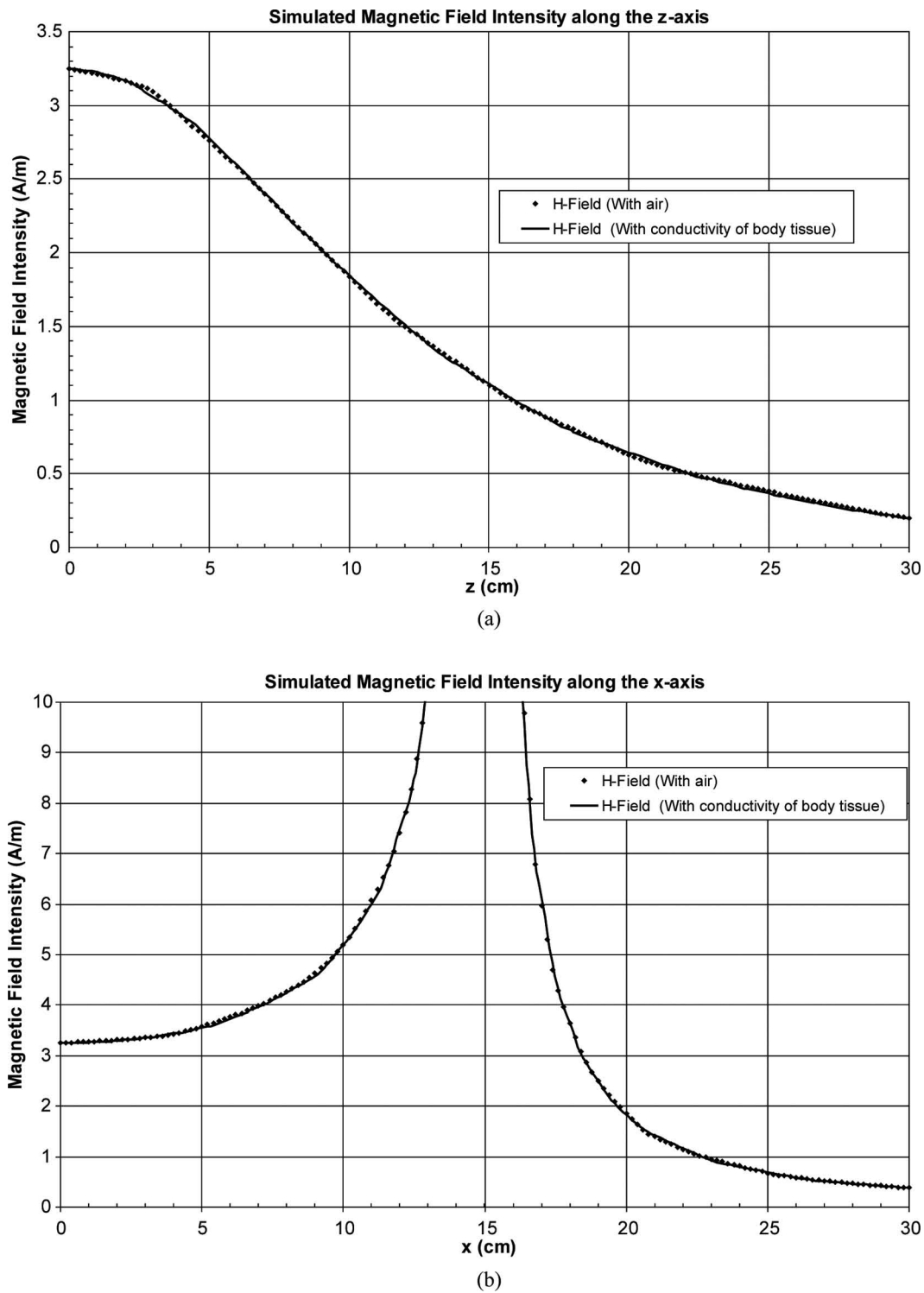


Fig. 2. Simulated magnetic field intensity along the (a) axial and (b) radial direction of a 30-cm-diameter current-carrying coil winding around cylinders filled with air and a material that has the same conductivity of physiology saline, mimicking the conductivity of body tissue.

ent parts of the circuit. Both the step-up and step-down converters are made of simple capacitor-diode networks, instead of buck or boost power converters which contain inductive components that are generally made of material which is not MR-compatible. Moreover, non-ferrite inductors which are MR compatible are not practical in boost converters, and are particularly unsuited for size-

restricted devices, because of their bulky size. Rather, in the present design, the receiving coil could come into close proximity with the primary coil wire. In that configuration, the induced voltage into the receiving coil could be significantly larger than normal. To prevent excessive current flow, a resettable fuse [22] in series with the resonating receiving coil can provide protection.

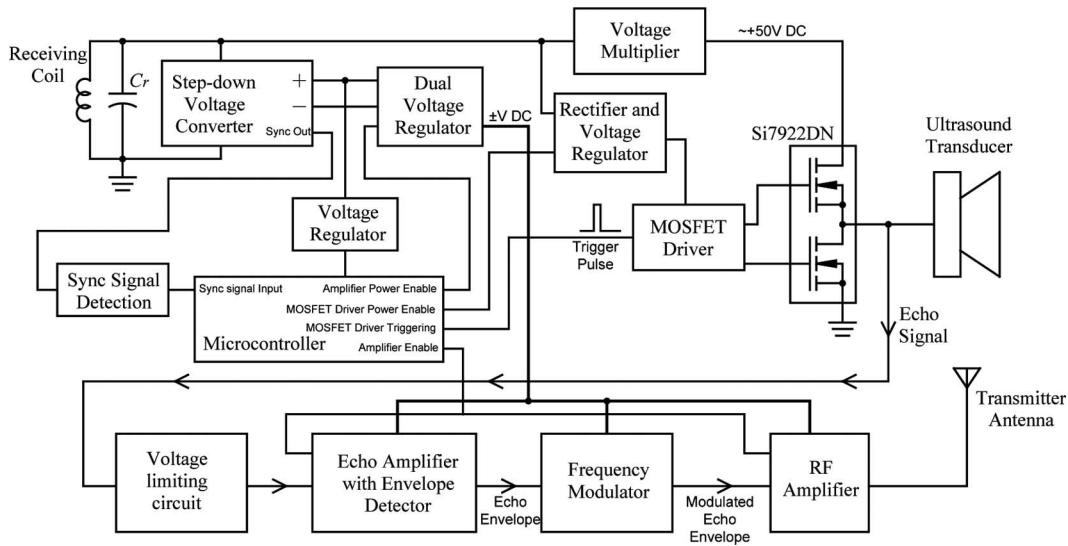


Fig. 3. A block diagram of the implanted device. Labeling of the MOSFET switch model is added for completeness.

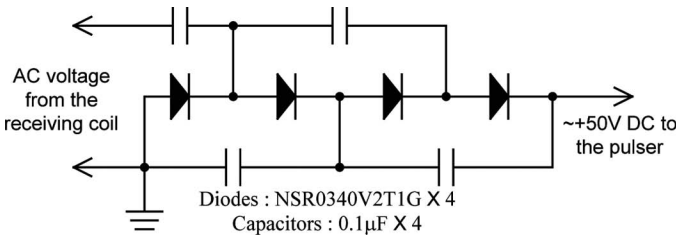


Fig. 4. A $4\times$ voltage multiplier used in the implantable device to boost the receiving coil voltage to about 50 V. Labeling of the diode model and capacitor sizes is added for completeness.

C. Pulser-Receiver Circuit

The operation sequence of each circuit module in the pulser-receiver and the pulser triggering are controlled by a microcontroller unit (MCU). In the prototype device shown in Fig. 3, a low-power consumption 8-bit MCU MC9S08 (Freescale Semiconductor inc., Austin, TX) is employed. The pulser is made of two MOSFETs in half-bridge configuration and generates a positive pulse with 50 V amplitude, 500 ns pulse width, and 10 Hz repetition frequency to drive a 5-MHz transducer. The transducer is used to convert the electrical pulse to a mechanical wave and also converts the ultrasound echo back into an electrical signal. The received signal from the transducer typically contains several oscillations at the transducer resonant frequency confined in an approximately Gaussian-shaped envelope. The received signal is amplified by 20 dB using an OPA890 operational amplifier in SOT-23 package from Texas Instruments (Dallas, TX) and its envelope is extracted by an envelope detector. The amplifier is protected by a voltage-limiting circuit to prevent it from being damaged by the high-voltage pulse generated by the pulser. The echo envelope is then modulated to 125-MHz carrier by a frequency modulator using a voltage-controlled oscillator (VCO). The modulated signal is amplified by 35 dB

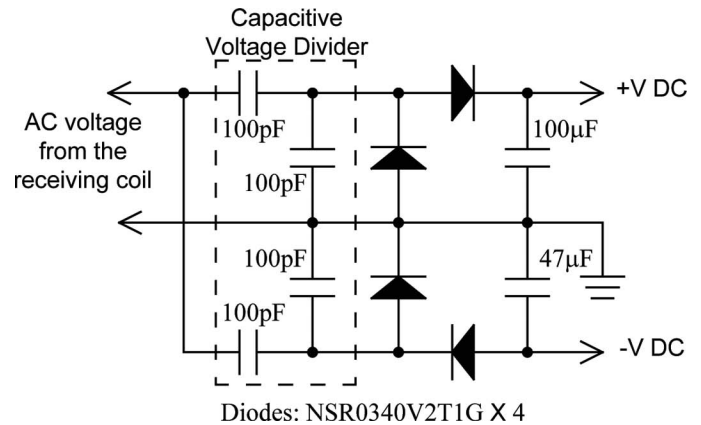


Fig. 5. A step-down voltage converter used to convert the receiving coil voltage to ± 6 V for the amplifiers and the microcontroller in the implantable circuit. Labeling of the diode model and capacitor sizes is added for completeness.

using a two-stage RF amplifier and transmitted through a monopole antenna with a length of about 4 cm.

D. Time Sequence of the Implantable Circuit

The whole implantable circuit operates inside a high-frequency current-carrying primary coil which generates a magnetic field for power transfer. This field may significantly interfere with the received ultrasound signal and the RF amplifier in the implantable circuit. To solve this potential problem, an idle time window for energy transfer is introduced when the ultrasound receiver is in operation. Inside this time window, the primary coil current and its induced magnetic field are temporarily turned off. The length of this time period is determined by the maximum detectable distance of the pulser-receiver system. In the system design, we set the maximum detectable object distance to be 15 cm. Because the speed of sound in soft tissue is about 1540 m/s, the corresponding time-of-flight

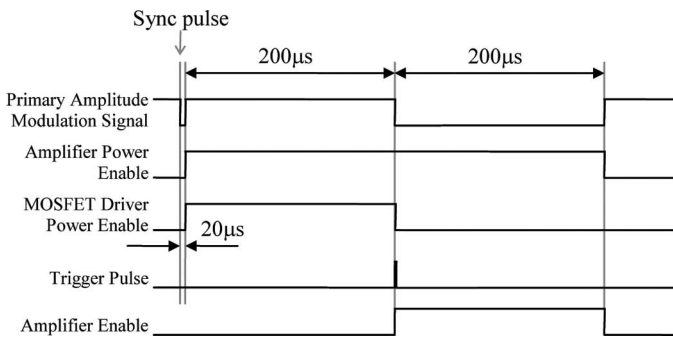


Fig. 6. Time sequence of the pulser-receiver system.

of the ultrasound signal is about $195 \mu\text{s}$. Therefore, the operating time period of the ultrasound receiver amplifier, which is the same as the idle time window for energy transfer, is set to $200 \mu\text{s}$.

As shown in Fig. 3, the timing signals are generated by a low-power-consumption microcontroller. The microcontroller operates continuously when it is supplied with sufficient power from the receiving coil. The power consumption of the microcontroller is about 12 mW . A $2.2\text{-}\mu\text{F}$ ceramic capacitor with a footprint of $1.6 \times 0.8 \text{ mm}^2$ is used to maintain a constant voltage during the idle time window. The implantable circuit sends and receives ultrasound signals 10 times every second and its operation is synchronized with the amplitude-modulated primary current. Fig. 6 shows the time sequence of each pulsing-receiving cycle. Each pulsing-receiving cycle is initiated by the sync pulse of the AM signal. After the implantable circuit is synchronized with the primary signal, the power regulators for supplying voltage to the amplifiers and the MOSFET driver in the implantable device are enabled. At $200 \mu\text{s}$ after the regulators are enabled, the pulser is triggered and sends a 50 V pulse to the ultrasound transducer. This $200 \mu\text{s}$ time period allows the regulator outputs to reach the desired voltage levels before the pulser and the receiver operates. The voltage regulator for the MOSFET driver is shut down after sending the pulse to save the energy received by the receiving coil. At the same time, the echo and RF amplifiers are enabled for $200 \mu\text{s}$. This $200 \mu\text{s}$ period is the same as the idle time window for the energy transfer from the primary coil. During this period, the ultrasound receiver picks up the echo signal, amplifies and extracts the echo envelope, and the echo envelope is frequency-modulated onto a carrier and transmitted out

to the external base receiver. After this period, the amplifiers and the voltage regulators are disabled once again and the capacitors at the rectifier outputs are charged for 99.58 ms before the next pulsing-receiving cycle.

IV. BASE STATION SIGNAL RECEIVER

The RF signal transmitted from the implantable circuit is received by a custom-made external base receiver located outside of and about 10 cm away from the primary coil. A monopole antenna with a length of approximately 10 cm is used to receive the RF signal. A parallel LC resonant network, which is comprised of an inductor, a fixed capacitor, and a variable capacitor, is used to increase the amplitude of the signal received from the base receiver antenna, as shown in Fig. 7. The resonant frequency of the LC network is adjusted to the carrier frequency of the modulated RF signal (125 MHz) by tuning the variable capacitor. The received RF signal is amplified by 70 dB with an RF amplifier and demodulated by a phase-locked loop (PLL). The high-frequency noise in the demodulated echo envelope signal is filtered out by a low-pass-filter with a cut-off frequency of 150 kHz . The echo envelope signal, with sufficiently high signal amplitude of 4 V maximum, is recovered at the output of the baseband amplifier.

V. TESTING AND VERIFICATION

A. Prototype Testing Setup

The wireless and batteryless pulser-receiver system was designed and implemented in-house. Both the implantable device and the external base receiver were made of off-the-shelf electronic components. The circuits were fabricated on double-sided printed-circuit-boards with a thickness of 0.8 mm . Surface-mounted components were adopted to reduce the size of the implantable device. The dimensions of the implantable circuit board (Fig. 8) are about $3 \times 3.8 \text{ cm}$. The implantable pulser was tested with a 5-MHz lead zirconate titanate planar ultrasound transducer with a diameter of 1 cm . The transducer was air-backed and fabricated in a water-proof protective housing. The ultrasound transducer was used both to generate an ultrasound wave and receive ultrasound echoes. During operation, the

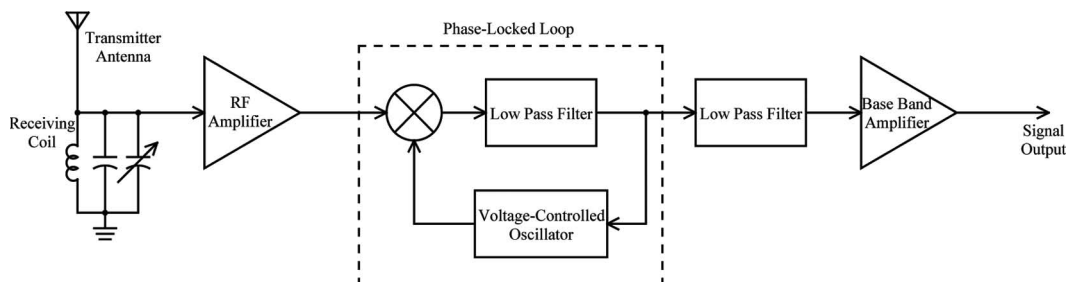


Fig. 7. A block diagram of the external base receiver.

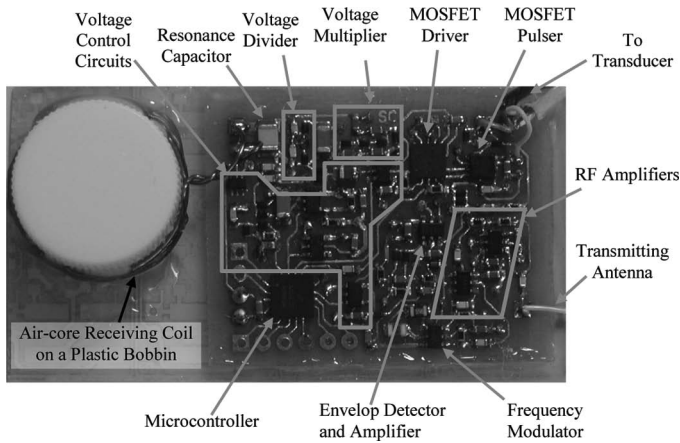


Fig. 8. A photograph of the implantable ultrasound pulser-receiver prototype.

receiving coil was placed at the center of the primary coil. The external base receiver was about 10 cm outside the primary coil. The diameter of the primary coil was 30 cm and the wire diameter was 0.5 mm. The excitation frequency of the primary current was 5.7 MHz. The amplitude-modulated primary current was set to 1.2 A rms to generate a pulse with 50 V in amplitude at the pulser output for the ultrasound transducer excitation. The amplitude and the width of the pulse generated by the pulser were about 50 V and 500 ns, respectively.

B. Bench-Top Prototype Verification

Fig. 9 shows the measured modulated primary coil current waveform, the sync signal demodulated from the receiving coil voltage, and the output waveforms of the voltage regulators for the amplifiers and the MOSFET driver in the implantable device. The waveforms were captured with an oscilloscope (Tektronix, DPO 3034, Beaverton, OR). When the microcontroller in the implantable device detected a sync pulse signal, it delivered turn-on signals to enable the voltage regulators for the amplifiers and the MOSFET driver. In this prototype, it took about 120 μs and 25 μs , respectively, for the voltage regulators for the amplifiers and the MOSFET driver to reach the desired output voltage levels. After a 200 μs period in which the implantable device was synchronized with the primary signal, the primary coil current excitation was then disabled for 200 μs . The energy-transfer idle time in the latter 200 μs period was intended to diminish the interference from the primary current to the ultrasound echo signal. The primary coil current resumed after the energy transmission idle time (200 μs) to charge up the rectifier capacitors for the next pulsing-receiving cycle. Meanwhile, the voltage regulators were disabled so that the amplifiers, modulation circuit, and the pulser did not consume the power being received by the receiving coil. When the regulator was disabled, the output voltages of

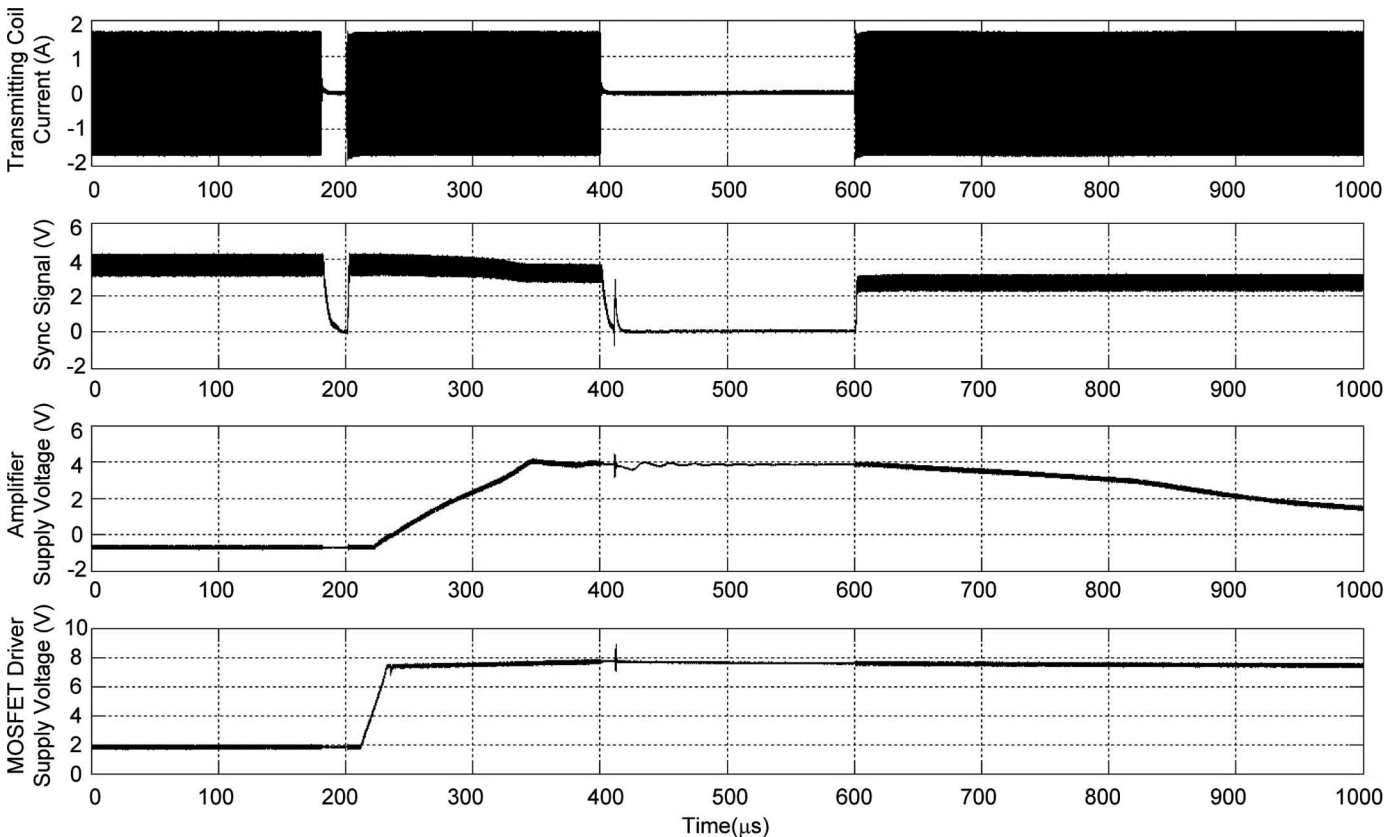


Fig. 9. Measured current of the primary coil, sync signal, amplifier supply voltage, and MOSFET driver supply voltage in the implantable device. The waveforms are replaced with those in which interfering noise sources are eliminated.

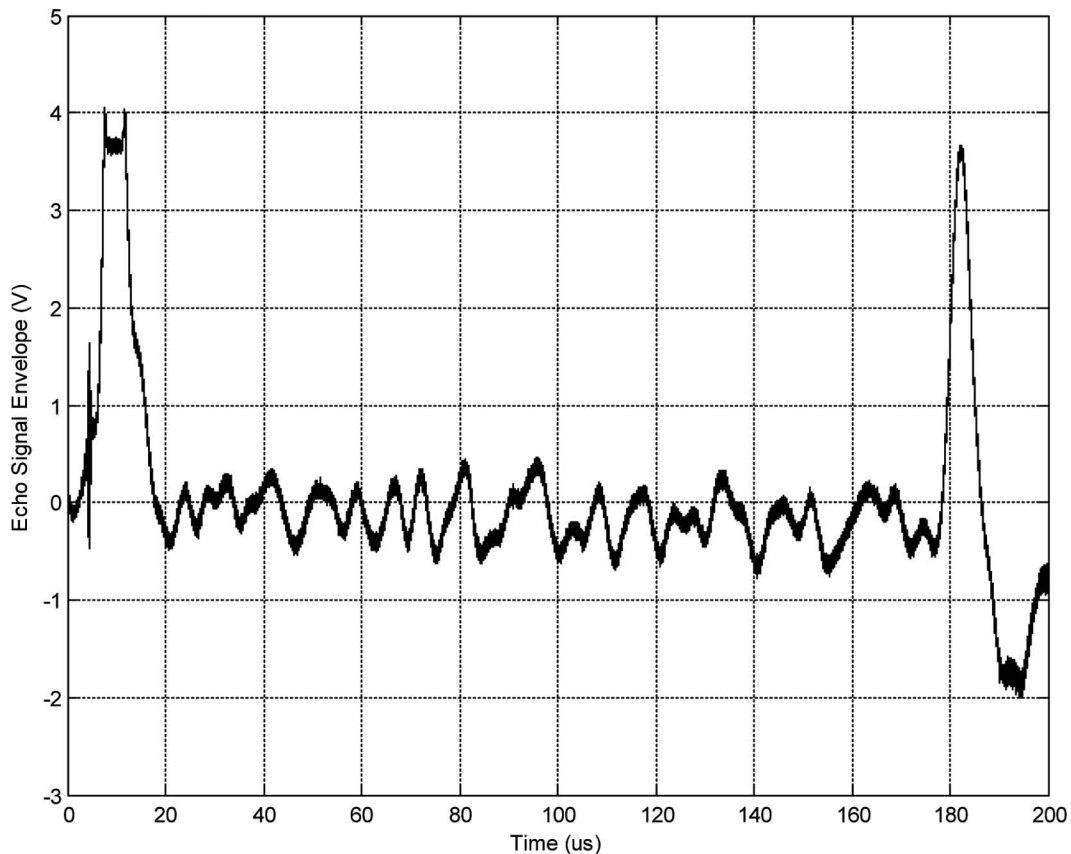


Fig. 10. Measured envelope voltage of the echo signal measured at the output of the base receiver.

the voltage regulators for the amplifier and the MOSFET driver were discharged as shown in Fig. 9. The discharging rate of the output of the regulator for the amplifiers was faster than that for the MOSFET driver, because the amplifiers shared the same power regulator with the modulator, which did not have an enable/disable function and its power consumption was higher than that of the MOSFET driver.

The system was tested by immersing the transducer in a water tank and aligning the transducer in parallel to the tank wall. The distance between the transducer and the wall was 12.5 cm. The transducer was connected with a coaxial cable to the implantable circuit, which was placed at the center of the primary coil. The base receiver was positioned about 10 cm from the primary coil. The tuning capacitor in the LC resonant network in the base receiver shown in Fig. 7 was adjusted to obtain the maximum signal amplitude at the RF amplifier output. The center frequency of the VCO in the phase-lock-loop was adjusted to the carrier frequency of the signal transmitted from the implantable circuit. The envelope of the echo signal received by the ultrasound transducer was reconstructed at the base receiver output and is shown in Fig. 10. The first pulse, with a peak of 4 V in the received signal, represents the envelope of the clamped pulser voltage in the implantable circuit when the transducer was excited with the 50 V pulse. The envelope of the ultrasound echo reflected from the tank wall was detected at 172 μs after the 50 V

pulse was sent to the transducer. Using a tabulated sound speed value of 1482 m/s, the calculated distance between the transducer and the tank wall is 12.7 cm, which agrees with the measured distance.

The effects of receiving coil placement error in the coil's axial and radial directions were examined. When the secondary receiving coil was situated on the plane and at the center of the primary coil, with their axes more or less parallel, the measured DC voltage at the voltage supply for the pulser was 50 V. When the receiving coil moved 5 cm away from the center in the radial direction, the measured supply voltage for the pulser varied less than 5 V. When the receiving coil moved 2 cm away from the primary coil center along the coil axis, a voltage drop of 1.2 V was observed. In other words, the received voltage had a secondary coil placement error of 2%/cm in the radial direction, and 1.2%/cm in the axial direction within ± 2 cm in radial and ± 5 cm in axial directions from the center of the primary coil.

C. Verification in an Ex Vivo Model

Design simulations predicted a negligible effect on the power transfer as a result of tissue conductivity. To verify this under more realistic conditions, measurements were acquired in a rabbit, *ex vivo*, to test the feasibility of energy transfer by magnetic coupling via conductive biological tissues. In this demonstration, the prototype circuit was

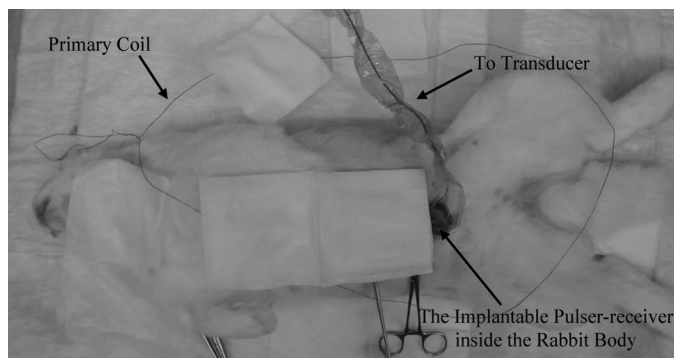


Fig. 11. A photograph showing the *ex vivo* rabbit experiment.

implanted and then operated inside the body of a rabbit (Fig. 11). The whole circuit was protected by a water resistant plastic membrane and placed into the abdominal cavity of the rabbit, under the large intestine and small intestine, and positioned on the surface of the posterior abdominal wall. The primary coil was put around the rabbit. The excitation current of the primary coil and the transducer setup were the same as those in the bench-top measurements. The DC voltage supplied to the pulser was measured and its value was found to be similar to that recorded in air without implantation. In addition, the envelope signal recorded at the output of the base receiver was found to be similar to bench-top measurements, as shown in Fig. 10.

VI. DISCUSSION

This study demonstrated the operation of a deep-seated implantable ultrasonic pulser-receiver powered wirelessly through magnetic coupling. The device starts to operate when the secondary coil receives sufficient power from the magnetic field generated by the primary current. The circuit was tested when the receiving coil was located on the plane and at the center of the primary coil. The separation between the two coil wires was about 14 cm, suggesting that the method can transfer energy wirelessly into a deep-seated circuit placed in the body. Because such an implantable device would not contain a battery, the device could be operated as needed over an indefinite period without the need for periodic battery replacement surgeries.

The implantable device design uses capacitor-diode networks to step up the voltage at the receiving coil from 12.5 to 50 V, allowing for ultrasound transducer excitation. Conversely, networks step down the voltage to about 6 V, which is then regulated to the desired voltage levels for the microcontroller and the amplifier circuits. The use of a capacitor-diode network, as opposed to more traditional buck and boost power converters, eliminates the use of ferromagnetic inductors, allowing the implantable device to be made MR-compatible. Likewise, the receiving coil is coreless and made of copper wire, so there is no ferromagnetic material involved in the energy-receiving

circuit. Thus, an MR-compatible implantable device can be achieved with the proposed energy transfer method.

One of the main advantages of using implanted device is to improve the signal integrity and the resolution of deep-seated tissue detection using a higher-frequency ultrasound, which is challenging when applied externally because of signal attenuation. The implantable pulser-receiver device was designed to monitor deep-seated tissue or organs that are surrounded by other tissues that high-frequency ultrasound cannot penetrate efficiently. Though not studied here, placement behind bone, including the skull bone, during surgery could provide a straightforward method for continuous monitoring in areas that are not readily accessible to ultrasound because of high beam attenuation [7].

The resonant frequency of the ultrasound transducer tested in this study is 5 MHz, so even for a high-Q transducer, selected for efficiency over bandwidth, 1 to 2 mm axial resolution would be expected, assuming up to a 6-cycle pulse length. This would be sufficient to detect abnormalities of the renal artery (typically 5 mm-diameter), which are characterized by greater than 50% change. Because overall kidney dimensions typically range 100 to 130 mm long and 50 to 70 mm in width, an exemplar 10-mm-diameter focused transducer with 75 mm radius of curvature, would produce an elongated beam (2-mm waist) with peak intensity near the center of the kidney (peak at 50 mm, -3 -dB 100 mm on-axis). Estimating a blood-kidney reflection coefficient of 5%, a 10% scattering cross-section, tissue absorption of 0.115 Np/cm, and transducer efficiency of 50%, received signals on the order of 1 to 10 mV might be expected in our operation range of 50 V. This order of magnitude is much higher than the sensitivity of the receiving circuit.

Results verified the design simulation's prediction that the magnetic field intensity around the center of the primary coil does not vary significantly along the coil axis and the maximum field occurs on the plane of the primary coil. This indicates that locating the receiving coil on the primary coil plane could result in optimal magnetic field coupling and also allows a few centimeters of coil placement error in the axial direction. These results also show that the magnetic field on the plane and around the center of the primary coil is approximately homogeneous and that the induced voltage at the receiving coil is not sensitive to the placement in the radial direction.

FEA magnetic field simulation also predicted that the effect of body tissue conductivity on the magnetic energy absorption would be negligible at the operation frequency of 5 MHz. This was verified by an *ex vivo* animal experiment. When implanted inside the abdomen of a rabbit, the implantable device displayed results comparable to operation in open air.

The operating frequency for energy transfer and the repetition frequency of the pulser-receiver were arbitrarily chosen in this study. A higher operating frequency for energy transfer could be chosen with the consideration of magnetic energy absorption in body tissue to minimize

the size of the energy-receiving coil. A lower pulser repetition frequency could also be selected to reduce the power consumption of the pulser, receiver, and the RF amplifiers to reduce the size of the receiving coil.

The implantable pulser-receiver circuit was implemented on a double-sided printed-circuit board (PCB) with off-the-shelf components with standard packages for experimental and demonstration purposes. Further work could be done on reducing the size of the implantable circuit by using a multilayer PCB and implementing some parts of the circuit, such as the pulser, amplifiers, and the modulator, into an integrated circuit. Likewise, the ultrasound transducer could be incorporated into the circuit by, for example, using a CMUT design [23]. The size of an optimized device could reasonably be on the order of one square centimeter.

VII. CONCLUSIONS

A wireless, batteryless deep-seated implantable ultrasonic pulser-receiver is demonstrated in this paper. The implantable device is powered by magnetic coupling between two co-planar coils. The primary coil, driven by a 5.7 MHz current, is designed to wrap around the body to generate magnetic field. The secondary coil is located near the center of and in the same plane as the primary coil to receive the magnetic energy and convert it to electrical energy for powering the implantable circuit. Both FEA simulation and experimental results show that the magnetic coupling is not sensitive to coil placement in either axial or radial directions. An *ex vivo* rabbit experiment was performed to verify the simulation to show that conductive biological tissues do not have obvious impact on the attenuation of the magnetic energy transfer, and the implantable device operated normally in both bench-top and *ex vivo* conditions.

The implantable pulser-receiver was tested with a 5-MHz ultrasound transducer in pulse-echo mode. The received echo reflected from the object to be detected was amplified, envelope-detected, modulated and transmitted outside the rabbit body through a radio wave. An external radio receiver was used to receive and demodulate the radio signal and recover the echo envelope. The distance between the transducer and the object was evaluated based on the arrival time of the echo signal recovered by the external receiver, and the evaluated result was consistent with the distance measurement. Further work is suggested for miniaturizing the implantable device by fabricating parts of the circuit into an integrated circuit and minimizing the receiving coil by increasing the magnetic field frequency with the consideration of energy absorption of body tissues.

REFERENCES

- [1] B. B. Lee, "Method and apparatus for monitoring heart function in a subcutaneously implanted device," U.S. Patent 7035684, Apr. 25, 2006.
- [2] B. Ferek-petric and B. Breyer, "Tricuspid flow synchronized cardiac electrotherapy system with blood flow measurement transducer and controlled pacing signals based on blood flow measurement," U.S. Patent 5243976, Sep. 14, 1993.
- [3] B. Ferek-petric and B. Breyer, "Ultrasound methods and implantable medical devices using same," U.S. Patent 7037266, May 2, 2006.
- [4] D. Vilkomerson and T. Chilipka, "Implantable Doppler system for self-monitoring vascular grafts," in *Proc. IEEE Ultrasonics Symp.*, 2004, vol. 1, pp. 461–465.
- [5] J. Chen, X. Cheng, P. Lin, and S. Zhou, "Implantable ultrasound emitter array for medical applications," in *Proc. IEEE Micro Electro Mechanical Systems*, 2006, pp. 422–425.
- [6] K. J. Parker, R. M. Lerner, and R. C. Waag, "Attenuation of ultrasound: Magnitude and frequency dependence for tissue characterization," *Radiology*, vol. 153, no. 3, pp. 785–788, 1984.
- [7] F. J. Fry and J. E. Barger, "Acoustical properties of the human skull," *J. Acoust. Soc. Am.*, vol. 63, no. 5, pp. 1576–1590, 1978.
- [8] M. R. Ardalan, M. K. Tarzamni, M. M. Shoja, R. S. Tubbs, B. Rahimi-Ardabili, K. Ghabili, and H. T. Khosroshahi, "Black tea improves endothelial function in renal transplant recipients," *Transplant. Proc.*, vol. 39, no. 4, pp. 1139–1142, 2007.
- [9] C. M. Rigsby, K. J. Taylor, G. Weltin, P. N. Burns, M. Bia, R. A. Princenthal, M. Kashgarian, and M. W. Flye, "Renal allografts in acute rejection: Evaluation using duplex sonography," *Radiology*, vol. 158, no. 2, pp. 375–378, 1986.
- [10] J. R. Salaman, "Monitoring of rejection in renal transplantation," *Immunol. Lett.*, vol. 29, no. 1–2, pp. 139–142, 1991.
- [11] D. Lagaaij, G. F. Cramer-Knijenburg, F. J. Kemenade, L. A. Es, J. A. Bruijn, and J. H. J. M. Krieken, "Endothelial cell chimerism after renal transplantation and vascular rejection," *Lancet*, vol. 357, no. 9249, pp. 33–37, 2001.
- [12] A. Irshad, S. J. Ackerman, A. S. Campbell, and M. Anis, "An overview of renal transplantation: Current practice and use of ultrasound," *Seminars in Ultrasound, CT, and MRI*, vol. 30, no. 4, pp. 298–314, 2009.
- [13] D. C. Galbraith, M. Soma, and R. L. White, "A wide-band efficient inductive transdermal power and data link with coupling insensitive gain," *IEEE Trans. Biomed. Eng.*, vol. 34, no. 4, pp. 265–275, 1987.
- [14] F. Zhang, X. Liu, S. A. Hackworth, R. J. Scabassi, and M. Sun, "Wireless energy delivery and data communication for biomedical sensors and implantable devices," in *Proc. IEEE Bioengineering Conf.*, 2009, pp. 1–2.
- [15] C. M. Zierhofer and E. S. Hochmair, "High-efficiency coupling-insensitive transcutaneous power and data transmission via an inductive link," *IEEE Trans. Biomed. Eng.*, vol. 37, no. 7, pp. 716–722, 1990.
- [16] C. M. Zierhofer and E. S. Hochmair, "Geometric approach for coupling enhancement of magnetically coupled coils," *IEEE Trans. Biomed. Eng.*, vol. 43, no. 7, pp. 708–714, 1996.
- [17] M. Soma, D. C. Galbraith, and R. L. White, "Radio-frequency coils in implantable devices: Misalignment analysis and design procedure," *IEEE Trans. Biomed. Eng.*, vol. 34, no. 4, pp. 276–282, 1987.
- [18] G. B. Joung and B. H. Cho, "An energy transmission system for an artificial heart using leakage inductance compensation of transcutaneous transformer," *IEEE Trans. Power Electron.*, vol. 13, no. 6, pp. 1013–1022, 1998.
- [19] X. Liu, F. Zhang, S. A. Hackworth, R. J. Scabassi, and M. Sun, "Wireless power transfer system design for implanted and worn devices," in *Proc. IEEE Bioengineering Conf.*, 2009, pp. 1–2.
- [20] E. S. Hochmair, "System optimization for improved accuracy in transcutaneous signal and power transmission," *IEEE Trans. Biomed. Eng.*, vol. 31, no. 2, pp. 177–186, 1984.
- [21] R. C. Lee, E. N. Bodnar, P. Betala, and S. Blom-Eberwein, "Electrical shock trauma," in *Handbook of Biological Effects of Electromagnetic Fields: Biological and Medical Aspects of Electromagnetic Fields*, 3rd ed., K. S. Barnes and B. Greenebaum, Boca Raton, FL: CRC, p. 335.
- [22] V. E. Stygar, J. E. Osuna, B. T. Pointer, and J. J. Ekis, "Resettable fuse," U.S. Patent 5963121, Oct. 5, 1999.
- [23] O. Oralkan, A. S. Ergun, J. A. Johnson, M. Karaman, U. Demirci, K. Kaviani, T. H. Lee, and B. T. Khuri-Yakub, "Capacitive micro-machined ultrasonic transducers: Next-generation arrays for acoustic imaging?" *IEEE Trans. Ultrason. Ferroelectr. Freq. Control*, vol. 49, no. 11, pp. 1596–1610, 2002.



Sai Chun Tang (S'97–M'01) was born in Hong Kong in 1972. He received the B.Eng. degree (with first class honours) and the Ph.D. degree in electronic engineering from the City University of Hong Kong in 1997 and 2000, respectively. After he graduated, he worked as a research fellow at the same university. He joined the National University of Ireland, Galway, as a visiting academic in 2001, and then the Laboratory for Electromagnetic and Electronic Systems at the Massachusetts Institute of Technology (MIT), Cambridge, in 2002. Since 2004, he has been working at the Fo-

cused Ultrasound Laboratory at Brigham and Women's Hospital, Harvard Medical School, Boston, MA, responsible for the developments of ultrasound diagnosis devices and non-invasive treatment systems using high-intensity focused ultrasound (HIFU). In 2008, Dr. Tang became an Instructor in Radiology at Harvard Medical School. His research interests involve high-frequency electromagnetism, low-profile power converter design, and analog electronics.

Ferenc A. Jolesz and **Gregory T. Clement** photographs and biographies were unavailable at the time of publication.